Light-Emitting Diodes

Deutsche Ausgabe: DOI: 10.1002/ange.201604427
Internationale Ausgabe: DOI: 10.1002/anie.201604427

Improvement of the Water Resistance of a Narrow-Band Red-Emitting $SrLiAl_3N_4:Eu^{2+}$ Phosphor Synthesized under High Isostatic Pressure through Coating with an Organosilica Layer

*Yi-Ting Tsai[+], Hoang-Duy Nguyen[+], Agata Lazarowska, Sebastian Mahlik, Marek Grinberg, and Ru-Shi Liu**

Abstract: *A $SrLiAl_3N_4:Eu^{2+}$ (SLA) red phosphor prepared through a high-pressure solid-state reaction was coated with an organosilica layer with a thickness of 400–600 nm to improve its water resistance. The observed $4f^65d \rightarrow 4f^7$ transition bands are thought to result from the existence of Eu^{2+} at two different Sr^{2+} sites. Luminescence spectra at 10 K revealed two zero-phonon lines at 15377 (for Eu(Sr1)) and 15780 cm^{-1} (for Eu(Sr2)). The phosphor exhibited stable red emission under high pressure up to 312 kbar. The configurational coordinate diagram gave a theoretical explanation for the $Eu^{2+/3+}$ result. The coated samples showed excellent moisture resistance while retaining an external quantum efficiency (EQE) of 70% of their initial EQE after aging for 5 days under harsh conditions. White-light-emitting diodes of the SLA red phosphor and a commercial $Y_3Al_5O_{12}:Ce^{3+}$ yellow phosphor on a blue InGaN chip showed high color rendition (CRI = 89, R9 = 69) and a low correlated color temperature of 2406 K.*

Most commercial white-light-emitting diodes (WLEDs) are fabricated on the basis of blue-LED chips and yellow-emitting $Y_3Al_5O_{12}:Ce^{3+}$ ($YAG:Ce^{3+}$) phosphors.[1,2] However, this approach limits the application to cool white light (correlated color temperature of 4000–8000 K) and the color-rendering index ($CRI < 75$).[3,4] Red-emitting materials, which are an important component for ideal white-LED fabrication, have attracted extensive attention recently. Nitride red phosphors are well-known and applied commercially because of their adequate luminescence efficiency and chemical strength. However, broad bands of emission restrict the maximum realizable luminous efficacies of high-quality warm WLEDs to an extremely large extent.[5–7] Narrow-band red-emitting nitridoaluminate $(Ca,Sr)LiAl_3N_4:Eu^{2+}$ phosphors with excellent luminescence properties have shown a significant improvement in the luminous efficacy and color rendition of WLEDs.[8,9] However, the impurity phases and moisture instability of the phosphors have restricted their use in optoelectronic devices. Although hydrophobic metal oxides and organic materials have been used to protect luminescent materials from a high-humidity atmosphere, instability and a decrease in the luminous efficacy of coated phosphors at high temperatures were observed.[10–13] To minimize the reduction in photoluminescence intensity, the coating materials should be optically transparent, cover the surface of phosphor particles homogeneously, and be high in thermal stability. Alkyl phosphates and organosilicas, which are advanced materials combining inorganic and organic species, could serve the requirements of the coating, such as low light scattering, organic-phase flexibility, and inorganic-glass strength and durability.[14–18]

In this study, the $SrLiAl_3N_4:Eu^{2+}$ red phosphor was synthesized by a solid-state reaction under a high pressure of 100 MPa. Two luminescence bands of $SrLiAl_3N_4:Eu^{2+}$ (SLA) were identified and are thought to originate from the Eu^{2+} ions in two different lattice sites. The excellent optical properties of SLA were discovered by using hydrostatic pressure as a powerful crystal-field-tuning tool. Furthermore, an organosilica layer on SLA rendered it waterproof and even enhanced its already efficient emission intensity and thermal properties.

The synchrotron X-ray diffraction (SXRD) patterns of the prepared SLA phosphors are shown in Figure 1 A. Crystallographic parameters from the Rietveld refinement gave the lattice constants $a = 5.8452(4)$, $b = 7.4770(5)$, and $c = 9.9214(6)$ Å. The obtained values matched well with the reported refined crystal structure of $SrLiAl_3N_4:Eu^{2+}$.[8] The diffraction pattern revealed a triclinic crystal structure that belongs to the P_1 space group. LiN_4 and AlN_4 tetrahedral sites are linked by corner-sharing N atoms, and channels of Sr centers along the [011] direction are coordinated within the LiN_4 and AlN_4 framework to form SrN_8 cuboid-like polyhedra (Figure 1 B). The photoluminescence excitation (PLE) spectrum of SLA at 654 nm is characterized by a broad band range of 400–650 nm, which is mainly due to the $4f^7(^8S_{7/2}) \rightarrow 4f^65d$ transition of Eu^{2+} ions.[19] The photoluminescence (PL) spectrum shows a narrow band with the maximum centered at 654 nm, which is ascribed to the Eu^{2+} transition from the lowest

[*] Dr. Y. T. Tsai,[+] Dr. H.-D. Nguyen,[+] Prof. Dr. R. S. Liu
Department of Chemistry, National Taiwan University
Taipei, 106 (Taiwan)
E-mail: rsliu@ntu.edu.tw
Prof. Dr. R. S. Liu
Department of Mechanical Engineering and Graduate Institute of Manufacturing Technology, National Taipei University of Technology
Taipei, 106 (Taiwan)
Dr. A. Lazarowska, Dr. S. Mahlik, Prof. Dr. M. Grinberg
Institute of Experimental Physics, University of Gdansk
Wita Stwosza 57, 80-952 Gdansk (Poland)
Dr. H.-D. Nguyen[+]
Institute of Applied Materials Science
Vietnam Academy of Science and Technology
Hochiminh City, 700000 (Vietnam)
[+] These authors contributed equally to this work.

Supporting information for this article can be found under: http://dx.doi.org/10.1002/anie.201604427.

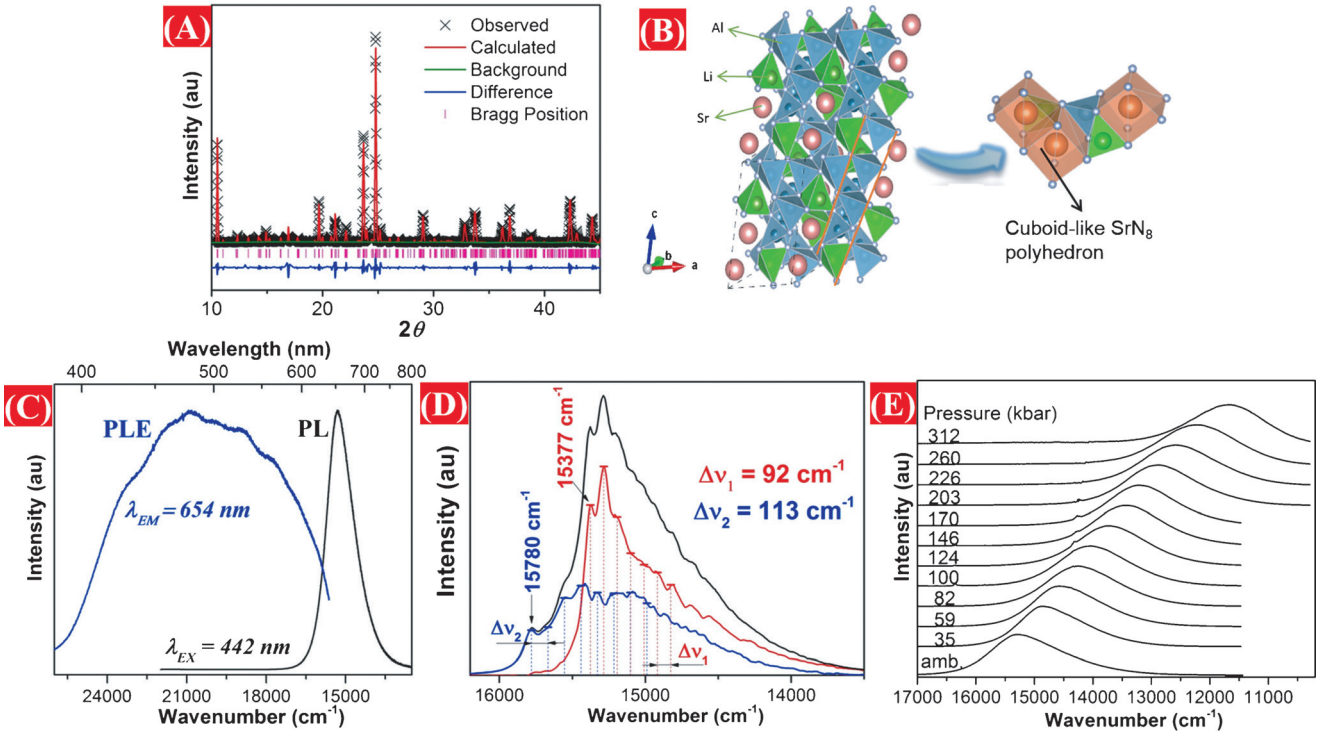

Figure 1. Structural and optical characterization of $SrLiAl_3N_4:Eu^{2+}$. A) Synchrotron X-ray diffraction patterns of the Rietveld refinement. B) Crystal structure. C) PLE spectrum (monitored at 654 nm) and PL spectrum (excitation at 442 nm). D) Deconvolution of the luminescence spectrum of SLA at 10 K, revealing two different emission centers with the zero-phonon line and calculated phonon energy. E) Room-temperature luminescence spectra of SLA under different hydrostatic pressures.

$4f^65d^1$ excited state to the $4f^7$ ($^8S_{7/2}$) ground state (Figure 1C). The relatively narrow PL band of SLA at room temperature (full-width half-maximum (FWHM): 1190 cm^{-1}) becomes increasingly narrow with decreasing temperature (see Figure S1 in the Supporting Information) as the vibronic structures of the emission transitions start to be resolved. Two different Sr^{2+} crystallographic sites are in the $SrLiAl_3N_4$ lattice, each coordinated by eight N atoms with an average Sr–N distance of 0.279 nm in a highly symmetric cuboid-like environment.

The Eu^{2+} activators can evenly occupy the two Sr^{2+} sites because of the similarity in their ionic radii; hence, broader emission-spectral overlaps of these two emission centers are observed. Nevertheless, these two centers have a different decay time and start to be distinguishable at 10 K (see Figure S2). By time-resolved luminescence, it is possible to decompose the vibronic structure of the emission transition for the two Eu^{2+} sites (Figure 1D). The zero-phonon line (ZPL) for a Eu(Sr1) site is observed at 15377 cm^{-1}, and the phonon energy from the separation of vibronic states is 92 cm^{-1} (red curve). For the Eu(Sr2) site, the ZPL energy is observed at 15780 cm^{-1}, and the phonon energy is 113 cm^{-1} (blue curve). The single-exponential decay of the 15377 cm^{-1} luminescence has a decay time of 0.65 μs. Meanwhile, the decay of the 15780 cm^{-1} luminescence deviates from a single exponential and is increasingly fast. Therefore, to calculate the average decay time (τ), the following formula was used:

$$\tau = \frac{\int I(t)tdt}{\int I(t)dt}$$

in which $I(t)$ is the intensity of luminescence. The obtained τ value for the 15780 cm^{-1} emission is 0.37 μs. The decay time varies across the emission band because the two emissions are superimposed in SLA. For Eu(Sr2), the decay time can only be distinguished at low temperatures below 150 K, and was found to be 0.37 μs. Above this temperature, the Eu(Sr2) decay time becomes impossible to determine owing to the strong overlap of the Eu(Sr1) and Eu(Sr2) emission. For Eu(Sr1), single-exponential decay curves were found at all considered temperatures (see Figure S3A for the luminescence decay time of the SLA as monitored at the maximum of luminescence versus temperature).

Room-temperature luminescence spectra of SLA under different hydrostatic pressures are presented in Figure 1E. Within the measured pressure range from ambient to 312 kbar, a redshift of the $4f^65d \rightarrow 4f^7$ emission band was observed because the rise of pressure causes an increase in the crystal-field strength.[20] The energy of the emission maximum shifts linearly with increasing pressure at a rate of $-11.6\ cm^{-1}\,kbar^{-1}$ (see Figure S3B). For all pressures, the decay of Eu(Sr1) luminescence was almost single-exponential (see Figure S4 for the pressure dependence of the decay as observed at the maximum of the emission band). The decay time increased slightly from 0.62 to 0.88 μs as the pressure increased from ambient pressure to 250 kbar. This behavior can be expected because pressure diminishes the energy of the lowest $4f^65d$ state with respect to the condution-band edge.[21] The luminescence decay time increases as the emission is red-shifted, which indicates that the emission of SLA is stable at all considered pressures.

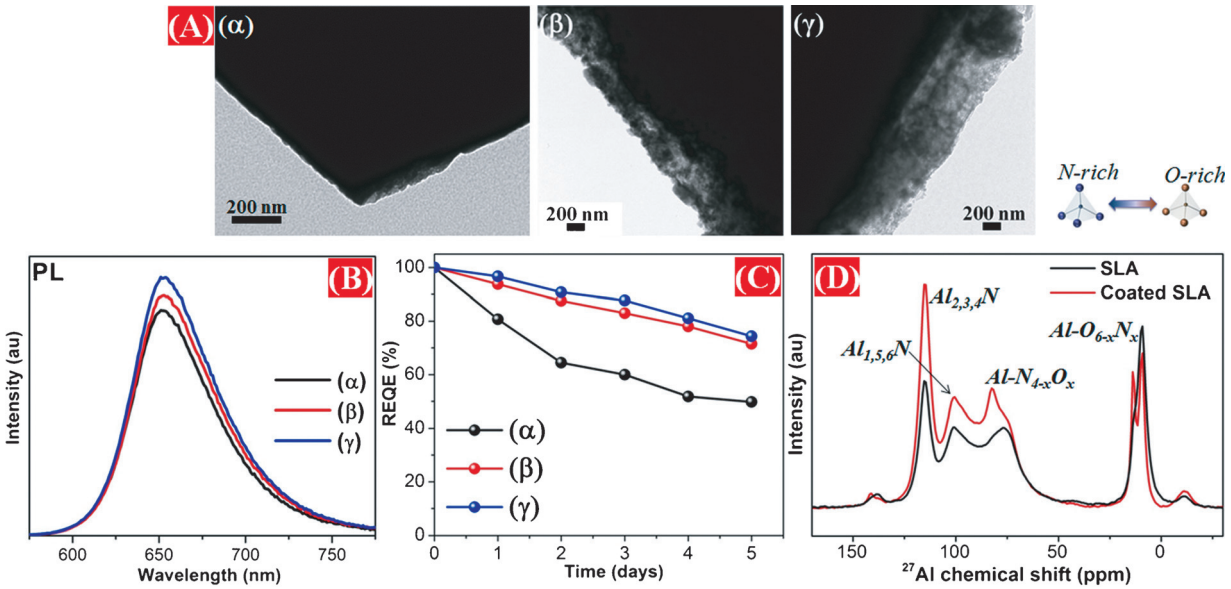

Figure 2. A) TEM images, B) PL spectra, and C) REQE of SLA with various TEOS contents: 0.0 (α), 3.0 (β), and 6.0 mM (γ). The internal and external QE were measured after aging under HT and HH conditions by excitation with 460 nm light. D) ^{27}Al solid-state NMR spectra showing the oxygen content in the cyrstal structure of SLA (black line) and coated SLA (red line).

The thickness of the OSi coating on the SLA surface was enhanced significantly from 400 to 600 nm with an increase in the tetraethylorthosilicate (TEOS) content from 3.0 to 6.0 mM, as confirmed by transmission electron microscopy (Figure 2 A). The morphology of coated-SLA and bare-SLA samples was observed by field-emission scanning electron microscopy (FESEM; see Figures S5). FTIR spectra of the coated-SLA samples showed bands at 2900–3000 cm^{-1} assigned to the C–H group vibration of TEOS and 3-(aminopropyl)trimethoxysilane, and bands at 1000–1100 cm^{-1} corresponding to the Si–O vibration (see Figure S6). A remarkable improvement in the emission intensity upon coating was observed (Figure 2 B). The EQE at room temperature of SLA and coated SLA prepared with 3.0 and 6.0 mM TEOS was 0.440, 0.505, and 0.521, respectively. The higher optical efficiency of coated samples might be due to their stability toward humidity. Figure 2 C shows the significant durability of coated SLA samples exposed to a harsh environment with 85% humidity at 85 °C for 5 days. The relative EQE ($REQE = EQE_t/EQE_{t=0}$) of coated SLA (3.0 mM TEOS) was significantly higher at 72% than that of SLA ($REQE \approx 50\%$) after 5 days under high-humidity and high-temperature conditions. A modest increase in the resistance of coated SLA to moisture with increasing TEOS content of up to 6.0 mM ($REQE \approx 75\%$) was observed (Figure 2 C).

SLA samples with and without a coating were studied by solid-state Li NMR spectroscopy at a rotation frequency of 20 MHz (see Figure S7). A split peak observed at 2.4/−0.1 ppm corresponds to two different Li sites in the SLA structure. No significant difference is present in the Li NMR spetra of the SLA samples because the LiN_4 tetrahedron is stable to oxygen.[21] Interesting distinctions were observed by Al NMR spectroscopy (Figure 2 D). The major peaks of the SLA samples occurred at 114 and 101 ppm, and are attributed to two groups of AlN_4 with six different Al sites in the lattice (see Figure S8). The range of 90–70 ppm contains peaks due to tetrahedral alumina $AlN_{4-x}O_x$ ($x = 1, 2, 3$) sites. The AlO_6 cluster with an oxygen-rich environment exhibits a diamagnetic peak close to 0 ppm.[22] The peaks of coated SLA samples showed a high chemical shift, at 83 and 13 ppm, as compared with those of uncoated samples at 76 and 9 ppm. The results indicated that the coating layer protected the SLA phosphor from oxidation by the surrounding atmosphere significantly. With 93% emission at 523 K, the PL intensity of the coated SLA sample was comparable to that at room temperature (95%), which proves that the coating improved thermal stability (see Figure S9 for temperature-dependent emission spectra and integrated PL intensity (I_{PL}/I_{PL303}) of the SLA samples at increasing temperatures between 303 and 573 K).

X-ray absorption spectroscopy (XAS) showed a high ratio of Eu^{3+}/Eu^{2+} in uncoated-SLA samples (Figure 3 A); however, only luminescence related to Eu^{2+} was observed (Figure 1 C). Although it probably contributes to absorption, Eu^{3+} does not provide luminescence. A correlation with the energetic structure of SLA doped with Eu^{2+} and Eu^{3+} can be invoked to account for this observation. The band gap of the SLA is relatively narrow, $E_g = 4.56$ eV (36780 cm^{-1}).[23] The appearance of Eu^{2+} PL indicates that the ground state of Eu^{2+} and the first excited state for the electronic configuration $4f^6 5d$ are located in the SLA band gap. The first bump in the PLE spectrum appears at an energy of 17700 cm^{-1}. The maximum of the Eu^{2+} luminescence band appears at 15300 cm^{-1}. This result that the energy of the $4f^6 5d$ configuration is located 16500 cm^{-1} above the ground state, which means that the Eu^{2+} ground state is located at least 16500 cm^{-1} below the conduction band. Therefore, the Eu^{2+} ground state should be located at most 20280 cm^{-1} above the valence-band edge. The schematic energetic structure of

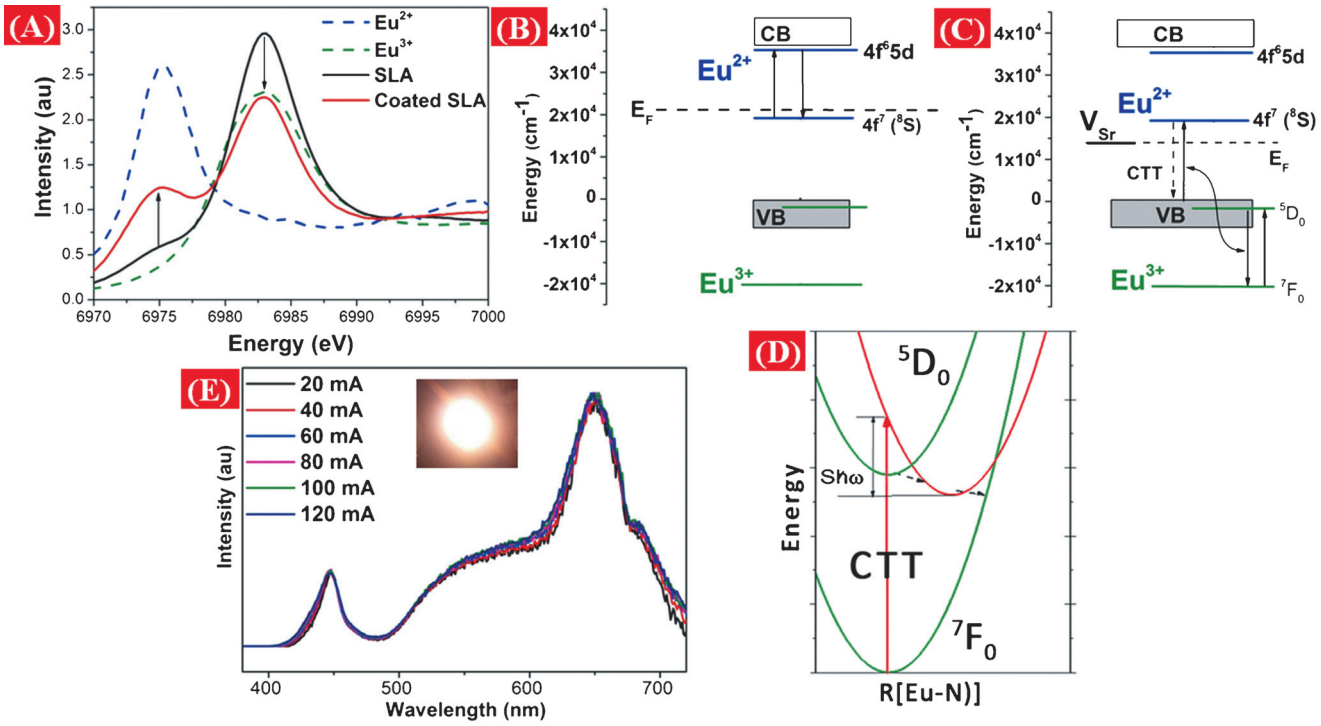

Figure 3. A) XAS spectra of Eu^{2+} (blue dashed line), Eu^{3+} (green dashed line), SLA (black line), and coated SLA (red line). B) Energetic structure (occupation diagram) of SLA:Eu^{2+}. C) Energetic structure (occupation diagram) of SLA:$Eu^{3+}+V_{Sr}$. D) Configurational coordinate diagram representing the real energetic structure of SLA:Eu^{3+}. E) PL spectra of WLEDs based on a blue-LED chip with YAG:Ce^{3+} and coated SLA under various drive currents. The inserted picture shows bright warm white light emitted from the fabricated WLEDs under a drive current of 20 mA.

SLA:Eu^{2+} is depicted in Figure 3B. The zero energy corresponds to the edge of the valence band of SLA. This occupation diagram (Figure 3B) can be considered in the same way as that of many electron systems (electrons in valence bands and $4f^7$ electrons of Eu^{2+}), whereby in the ground state of the entire SLA:Eu^{2+} system and the ground state of Eu^{2+} (^8S) are the highest occupied levels, and the energy of these states determines the location of the Fermi level in the band gap.

The energy of the ground state of Eu^{3+} is located below that of Eu^{2+} by approximately 5–7 eV (40300–56500 cm^{-1}) because the ionization energy of Eu^{3+} is considerably higher than that of Eu^{2+}.[24,25] In Figure 3B, this energy is equal to 40000 cm^{-1}, and the Fermi level of SLA with Eu is located above or is equal to the ground state of Eu^{2+}. Thus, this state is occupied, and d–f luminescence related to Eu^{2+} is observed (see arrows in Figure 3B). In some Eu sites, the energy of the Fermi level can be located below the ground state of Eu^{2+} owing to the appearance of a strontium vacancy, which creates donor levels in the band gap. In such sites, the ground state of Eu^{2+} is unoccupied, and the Eu ion exists as Eu^{3+} (see Figure 3C). Such sites can not contribute to the Eu^{2+} luminescence. They could potentially yield Eu^{3+} emission.[26,27] The Eu^{3+} species in these sites can be excited by f–f transitions or a charge-transfer transition (CTT): a transition of electrons from the valence band (VB) to Eu^{3+} (represented by the arrow labeled CTT in Figure 3C) to form Eu^{2+} and a hole in the valence band. The Eu^{3+} luminescence can be observed when the energy of the charge-transfer state (CT) is higher than the energies of excited emitting states of Eu^{3+}: ^5D_J, $J=0,1,2,3$. The energy of the $^5D_0$ state is approximately equal to 17000 cm^{-1}, and the predicted energy of CT is 20280 cm^{-1}. CT is characterized by a large lattice relaxation labeled $S\hbar\omega$ in Figure 3D, in which $\hbar\omega$ is the phonon energy and S is the Huang–Rhys factor, with a typical value of 5000 cm^{-1}. The situation is described by a configurational coordinate diagram of the SLA:Eu^{3+} system in Figure 3D. Lattice relaxation diminishes the energy of the CT state below the energy of the $^5D_0$ state. As a result of a large lattice relaxation, the excited SLA:Eu^{3+} system is seen to relax nonradiatively to the ground state of Eu^{3+} independently if Eu^{3+} is excited by CTT or directly to the $^5D_0$ state. The lower Eu^{3+}/Eu^{2+} ratio observed in coated SLA samples confirmed the importance of waterproof OSi shell layers.

WLEDs were fabricated from blue InGaN chips, a commercially available YAG:Ce^{3+} yellow phosphor, and a coated-SLA red phosphor. The narrow emission of SLA was observed in electroluminescent spectra of the WLEDs under various drive currents (Figure 3E). When the drive current was decreased from 120 to 20 mA, the luminous efficacy of the WLED was observed to increase from 59 to 76 lm W^{-1}. This result can be attributed to the large EQE of the blue chip under lower drive-current densities.[28] Thus, high-performance warm WLEDs with high CRIs ($R_a=89$–91, $R9=69$–71) were obtained (see Table S1 in the Supporting Information). In the Commission Internationale de l'Éclairage (CIE) 1931 color spaces, chromaticity coordinates (0.4609, 0.3764) and (0.4720, 0.3932) were plotted in close proximity to the black body locus. Furthermore, correlated color temperatures (CCTs) at 2413 and 2406 K were also

measured for WLEDs containing (YAG and SLA) and (YAG and coated-SLA), whereas the WLEDs that used only YAG showed a high CCT of 6000 K and a chromaticity coordinate of (0.3043, 0.3017; see Figure S10).

In summary, SLA red phosphors were prepared by a high-pressure solid-state reaction. At room temperature, the phosphor exhibits a broad PL band due to the $4f^6 5d \rightarrow 4f^7$ transition in Eu^{2+}, originating from the substitution of Eu^{2+} ions in two different Sr^{2+} sites, which are stable under high-pressure conditions up to 312 kbar. A significant enhancement (by about 25%) was observed in the EQE of coated phosphors as compared to that of uncoated samples. Moreover, the coated samples exhibited excellent moisture resistance with about 75% of the EQE remaining after aging for 5 days in high humidity (85%) at a high temperature (85°C). A warm WLED made from the coated-SLA red phosphor and commercial YAG:Ce^{3+} yellow phosphor on a blue InGaN chip was shown to possess a high CRI ($R_a = 89$, $R9 = 69$) and a low CCT of 2406 K. The results indicated that the $SrLiAl_3N_4$:Eu^{2+} coated with organosilica is a promising candidate for applications in warm WLED and field-emission light sources.

Acknowledgements

This research was supported by the Ministry of Science and Technology of Taiwan (Contract Nos. MOST 104-2113-M-002-012-MY3, MOST 104-2119-M-002-027-MY3, and MOST 104-2923-M-002-007-MY3) and Mitsubishi Chemical Group, Science and Technology Research Center Inc., Japan. We also appreciate the discussions with Dr. Kyota Ueda. The National Center for Research and Development Poland also provided financial support (Grant No. PL-TW2/8/2015). The contribution of S.M. was supported by the grant "Iuventus Plus" 0271/IP3/2015/73 from the Ministry of Science and Higher Education of Poland.

Keywords: charge transfer · coatings · light-emitting diodes · luminescence · phosphors

How to cite: *Angew. Chem. Int. Ed.* **2016**, *55*, 9652–9656
Angew. Chem. **2016**, *128*, 9804–9808

[1] R. Zhang, H. Lin, Y. Yu, D. Chen, J. Xu, Y. Wang, *Laser Photonics Rev.* **2014**, *8*, 158.
[2] C. C. Lin, R. S. Liu, *J. Phys. Chem. Lett.* **2011**, *2*, 1268.
[3] N. C. George, K. A. Denault, R. Seshadri, *Annu. Rev. Mater. Res.* **2013**, *43*, 481.
[4] M. R. Krames, O. B. Shchekin, R. Mueller-Mach, G. O. Mueller, L. Zhou, G. Harbers, M. G. Craford, *J. Disp. Technol.* **2007**, *3*, 160.
[5] R.-J. Xie, N. Hirosaki, Y. Li, T. Takeda, *Materials* **2010**, *3*, 3777.
[6] H. Nersisyan, H. I. Won, C. W. Won, *Chem. Commun.* **2011**, *47*, 11897.
[7] K. Uheda, N. Hirosaki, Y. Yamamoto, A. Naito, T. Nakajima, H. Yamamoto, *Electrochem. Solid-State Lett.* **2006**, *9*, H22.
[8] P. Pust, V. Weiler, C. Hecht, A. Tücks, A. S. Wochnik, A.-K. Henss, D. Wiechert, C. Scheu, P. J. Schmidt, W. Schnick, *Nat. Mater.* **2014**, *13*, 891.
[9] P. Pust, F. Hintze, C. Hecht, V. Weiler, A. Locher, D. Zitnanska, S. Harm, D. Wiechert, P. J. Schmidt, W. Schnick, *Chem. Mater.* **2014**, *26*, 6113.
[10] C. Zhang, T. Uchikoshi, L. Liu, Y. Sakka, N. Hirosaki, *Materials* **2014**, *7*, 3623.
[11] J.-H. Seo, S.-M. Lee, H.-S. Moon, S.-J. Han, S.-H. Sohn, *Mol. Cryst. Liq. Cryst.* **2010**, *531*, 82.
[12] H. S. Do, E. J. Kim, S. H. Hong, *J. Lumin.* **2010**, *130*, 1400.
[13] J. Zhuang, Z. Xia, H. Liu, Z. Zhang, L. Liao, *Appl. Surf. Sci.* **2011**, *257*, 4350.
[14] H. D. Nguyen, C. C. Lin, R. S. Liu, *Angew. Chem. Int. Ed.* **2015**, *54*, 10862; *Angew. Chem.* **2015**, *127*, 11012.
[15] W. Zhang, Y. Hu, J. Ge, H. L. Jiang, S. H. Yu, *J. Am. Chem. Soc.* **2014**, *136*, 16978.
[16] S. J. Yuan, S. O. Pehkonen, Y. P. Ting, K. G. Neoh, E. T. Kang, *ACS Appl. Mater. Interfaces* **2009**, *1*, 640.
[17] M. Pagliaro, R. Ciriminna, G. Palmisano, *J. Mater. Chem.* **2009**, *19*, 3116.
[18] I. Pastoriza-Santos, D. Gomez, J. Pérez-Juste, L. M. Liz-Marzán, P. Mulvaney, *Phys. Chem. Chem. Phys.* **2004**, *6*, 5056.
[19] W. M. Yen, S. Shionoya, H. Yamamoto, *Phosphors Handbook*, CRC Press, New York, NY, **1998**.
[20] M. Grinberg, *J. Lumin.* **2011**, *131*, 433.
[21] S. Mahlik, A. Lazarowska, J. Ueda, S. Tanabe, M. Grinberg, *Phys. Chem. Chem. Phys.* **2016**, *18*, 6683.
[22] J. J. Fitzgerald, *Solid-State NMR Spectroscopy of Inorganic Materials*, American Chemical Society, Washington, DC, **1999**.
[23] T. M. Tolhurst, T. D. Boyko, P. Pust, N. W. Johnson, W. Schnick, A. Moewes, *Adv. Opt. Mater.* **2015**, *3*, 546.
[24] P. Dorenbos, *J. Phys. Condens. Matter* **2003**, *15*, 8417.
[25] P. Dorenbos, *Phys. Rev. B* **2012**, *85*, 165107.
[26] A. Baran, J. Barzowska, M. Grinberg, S. Mahlik, K. Szczodrowski, Y. Zorenko, *Opt. Mater.* **2013**, *35*, 2107.
[27] A. Baran, S. Mahlik, M. Grinberg, P. Cai, S. I. Kim, H. J. Seo, *J. Phys. Condens. Matter* **2014**, *26*, 385401.
[28] H. M. Zhu, C. C. Lin, W. Luo, S. T. Shu, Z. G. Liu, M. Wang, J. T. Kong, E. Ma, Y. Cao, R. S. Liu, X. Y. Chen, *Nat. Commun.* **2014**, *5*, 4312.

Received: May 6, 2016
Published online: July 4, 2016

